Accepted Manuscript

Heterogeneously catalyzed two-step cascade electrochemical reduction of CO_2 to ethanol

Nolan Theaker, Jacob M. Strain, Bijandra Kumar, J. Patrick Brian, Sudesh Kumari, Joshua M. Spurgeon

PII: S0013-4686(18)30816-8

DOI: 10.1016/j.electacta.2018.04.072

Reference: EA 31639

To appear in: *Electrochimica Acta*

Received Date: 21 November 2017

Revised Date: 20 March 2018

Accepted Date: 10 April 2018

Please cite this article as: N. Theaker, J.M. Strain, B. Kumar, J.P. Brian, S. Kumari, J.M. Spurgeon, Heterogeneously catalyzed two-step cascade electrochemical reduction of CO_2 to ethanol, *Electrochimica Acta* (2018), doi: 10.1016/j.electacta.2018.04.072.

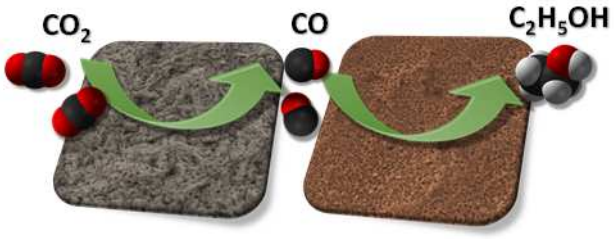

Heterogeneously Catalyzed Two-step Cascade Electrochemical Reduction of CO_2 to Ethanol

Nolan Theaker, Jacob M. Strain, Bijandra Kumar, J. Patrick Brian, Sudesh Kumari, and Joshua M. Spurgeon*

Conn Center for Renewable Energy Research, University of Louisville, Louisville, Kentucky, 40292, USA.

*Corresponding author. E-mail: joshua.spurgeon@louisville.edu

Abstract: Electrochemical reduction of CO_2 to liquid fuels is a promising route to a carbon-neutral, energy-dense storage of intermittent renewable electricity. However, electrocatalysts generally suffer from high overpotential and poor selectivity for multi-carbon products such as ethanol, and efforts to enhance such catalysts are limited by scaling relations which inhibit a simultaneous optimization of each elementary electrochemical step. In this work, the multistep proton-coupled electron-transfer reaction for the conversion of CO_2 to C_2H_5OH was strategically divided into two independently optimized steps in a sequential cascade reaction using heterogeneous electrocatalysts to convert CO_2 to CO and CO to C_2H_5OH within a single integrated electrochemical system. The exclusion of CO_2 reactant from the second-stage electrolyzer was observed to be critical for maintaining appreciable ethanol selectivity. The cascade system produced C_2H_5OH at an overall faradaic efficiency of 11.0% at an average applied potential of -0.52 V vs. RHE, making it highly competitive with known single-step electrocatalysts for ethanol production from CO_2. This performance was despite limited conversion of the intermediate CO between cascade steps (~6.4%), and reactor design improvements to enhance the conversion could lead to significantly enhanced ethanol production performance.

Keywords: CO_2 reduction, cascade catalysis, ethanol, liquid fuel, electrochemistry

1. Introduction

One promising solution for the energy storage of intermittent renewable electricity sources is to store the energy in the form of chemical bonds, i.e., to convert sunlight and wind to energy-dense fuels [1-3]. In addition to enabling more reliable utilities with longer term seasonal energy storage, conversion to fuels has the added benefit of concentrating these diffuse, renewable sources into a portable form suitable for transportation applications. The electrolysis of water to produce hydrogen fuel and the reduction of carbon dioxide with water to produce hydrocarbons are feasible processes to accomplish this energy storage at the terawatt scale. Liquid hydrocarbons such as ethanol have the advantage of a high volumetric energy density (24 MJ/L for C_2H_5OH) which is greater than compressed H_2 or the most advanced battery technologies [4]. Furthermore, electrolytic CO_2 reduction to fuels is a carbon-neutral process, contributing to sustainability and helping to mitigate potential climate change. Significant effort has thus been devoted in recent years to the direct conversion of sunlight into energy-dense fuels via the reduction of CO_2,[5-12] however, catalytic advances are still strongly needed to improve the prospects of this technology.

Unlike the hydrogen evolution reaction (HER), many different products are possible in the carbon dioxide reduction reaction (CO2RR) coupled with the oxidation of water [12-14]. Most metallic electrocatalysts only yield C_1 products [14-16], but copper surfaces are capable of directing significant faradaic current to C-C bond forming reactions and producing C_2 and C_3 products [17-21]. While there has been success at achieving high yields of CO [22-25] and formate [26-32] in a single-step CO_2 reduction process, more energy-dense fuel products such as ethanol have been difficult to produce with high faradaic efficiency and reproducibility [18-20].

Several efforts to develop electrocatalysts for a direct conversion of CO_2 to C_2H_5OH have shown reasonable faradaic efficiencies but generally required high overpotentials [33-39]. The CO2RR activity of single crystal planes of Cu have been reported with distinctly different activity to polycrystalline Cu, with a faradaic efficiency for C_2H_5OH as high as 29.9% for Cu(310), albeit with a high overpotential of > 1 V [34]. Cu surface orientations have also been observed to restructure under electrolysis conditions [40], adding uncertainty to the stability of a Cu single crystal catalyst. Additionally, oxide-derived Cu electrodes with varied oxide layer thicknesses led to C_2H_5OH faradaic efficiencies up to 16.4%, but again with an overpotential of ~ 1 V [35]. A recent report even claims C_2H_5OH faradaic efficiency up to 63% on Cu nanoparticles on graphene, but in a narrow potential range with cathodic overpotential upwards of 1.3 V [39].

The myriad possible reaction pathways on the way to C_2 and C_3 compounds underscores the difficulty of achieving high product selectivity in a single reaction step [18]. Theory and DFT calculations which have provided CO2RR mechanistic insight suggest that the optimal catalytic surface for driving a specific reaction pathway is one in which the free energy change of the reaction is achieved in thermochemically equivalent elementary steps [21]. However, changing the surface binding energy to tune the free energy of one elementary step has a concomitant effect on the free energy of the other elementary steps. Breaking this scaling relation is thus a major challenge to optimize electrocatalysis for CO2RR products such as C_2H_5OH and may be exceptionally difficult for one electrocatalyst in a single-step electrolysis [41]. Therefore, the field of electrolytic CO_2 reduction would benefit greatly from the development of approaches and systems to optimize the selectivity and overpotential of heterogeneous catalysts to more complex, desirable fuel products.

One approach to directing CO_2 reduction toward a more energy-dense product is to break

down the complex electron transfer reaction into multiple reaction steps with fewer electron transfers and relatively stable products. In this type of cascade catalysis, the products of the first reaction become the reactants of the second reaction, and so on, allowing for the design of multiple catalysts to minimize the energy barrier of each intermediate reaction on the way to the ultimately desired product. The advantages of cascade catalysis to improve product yield have been demonstrated in a "one-pot synthesis" for homogeneous catalysis of CO_2 to CH_3OH, using three different catalysts simultaneously to promote the conversion [42]. A major difficulty with the one-pot cascade is finding compatible catalysts that operate effectively under the same reaction conditions and are not poisoned by any of the intermediates.

Alternatively, an assembly line cascade system with stepwise reactors can be used with varying conditions tailored to optimize the kinetic rate and selectivity at each stage. The major advantage of an assembly line cascade is versatility and modularity. Each individual reaction can be operated with the optimal choice of catalyst, temperature, applied bias, etc., to maximize yield and minimize overpotential. While CO_2 conversion via heterogeneous cascade catalysis has been reported for thermochemical synthesis [43], reports for electrochemical CO_2 reduction are lacking. This versatile systems engineering approach could provide a framework to improve the selectivity of CO_2 electroreduction to higher order products.

Herein the viability of multistage cascade electrolysis to produce C_2H_5OH from CO_2 was demonstrated. The overall cathode half-reaction for ethanol formation is [33]:

$$2CO_2 + 9H_2O + 12e^- \rightarrow C_2H_5OH + 12OH^-,\ E^o = 0.09\ \text{V vs. RHE} \quad (1)$$

Ethanol production was pursued by splitting this reaction into two distinct electrochemical steps. For the assembly cascade approach, the intermediate product should be a stable species that is readily separated from the first electrolyte. CO, which has routinely been

demonstrated at high faradaic efficiencies from CO_2 electroreduction, was targeted as the stable intermediate product from the first stage [44]:

$$CO_2 + H_2O + 2e^- \rightarrow CO + 2OH^-,\ E^o = -0.10\ \text{V vs. RHE}$$

(2)

The low solubility of CO also makes it an easily separated intermediate product for passing to the second-stage electrolyzer, although it also presents a challenge to achieving subsequent high current density for CO reduction. Among numerous electrocatalytic systems which have shown high selectivity for CO formation, etched Ag nanocoral (Ag-NC) films have achieved > 95% faradaic efficiency at only -0.5 V vs. RHE in aqueous media with promising stability [45]. Furthermore, oxide-derived nanocrystalline Cu (OD-Cu) catalysts have reduced CO to C_2H_5OH at ~ 43% faradaic efficiency at only -0.3 V vs. RHE following the reaction [46]:

$$2CO + 7H_2O + 8e^- \rightarrow CH_3CH_2OH + 8OH^-,\ E^o = 0.18\ \text{V vs. RHE}$$

(3)

These catalytic systems were leveraged to demonstrate the cascade approach as a rational strategy for targeting high faradaic efficiency of a complex product at a low overall overpotential.

2. Experimental

2.1. Electrode Preparation. Ag-NC foil was used as the CO2RR catalyst for the first-stage electrolysis cell, along with an OD-Cu foil electrode for the second-stage electrolysis cell. The Ag-NC was prepared from a Ag foil (99.999% pure, Alfa Aesar) by first producing a AgCl surface by electrochemical oxidation at 0.3 V vs. Ag/AgCl in 0.1 M KCl electrolyte for 12 h. Subsequently, the foil was reduced to nanocoral structure by applying a potential of -1.2 V vs.

Ag/AgCl in the same electrolyte for 30 min [45].

The OD-Cu electrode was fabricated from a Cu foil (99.98% pure, Alfa Aesar) which was cleaned with a 1 M HCl soak for 2 minutes, then rinsed with isopropyl alcohol and water. The Cu foil was then dried with N_2 gas (99.99% pure) and then heated at 500 °C for 1 h under atmospheric air. Following thermal oxidation, the foil was cooled gradually to room temperature over ~ 1 h to prevent delamination of the oxide layer. The thermally oxidized Cu foil was electrochemically reduced at -0.6 V vs. RHE in 0.1 M KOH solution for 45 min. After the reduction process, fresh electrolyte was added to the cell prior to CO reduction [46].

2.2. Cascade Electrolyzer Design. The generalized layout of the cascade system is depicted in the schematic of Figure 1. CO_2 (99.99%, Specialty Gases) was flowed at 20 sccm with a mass flow controller (MKS Instruments, Inc.) through a custom absorption column filled with 0.1 M $KHCO_3$ in 18 MΩ-cm water in a random packing of 1 mm diameter glass beads. The liquid electrolyte was cycled with a peristaltic pump through the column and the cathode section of the first electrolyzer at a rate of 80 mL min^{-1}. The flow rates were chosen to provide near saturation of CO_2 in the electrolyte at the column outlet and to avoid transferring gaseous CO_2 bubbles to the first-stage electrolyzer. From the cathode (Ag-NC) of the first electrolysis cell, the electrolyte flowed into a separate chamber for an extended residence time, permitting the effective separation of product CO and H_2 bubbles from the liquid, with the electrolyte recycled back to the inlet of the CO_2 absorption column. The gaseous product output from the separation chamber of the first-stage electrolyzer was directed to the second-stage electrolyzer through a porous glass frit bubbler positioned at the bottom of the 0.1 M KOH catholyte to promote gas dissolution and mass transfer to the OD-Cu cathode. There was no pump in between the electrolyzer stages, with the evolution of gases in the first stage being the driver for gaseous flow. To avoid interruption of

the development of steady state conditions in the second-stage electrolyzer, gaseous products from the first-stage electrolyzer were not sampled by GC during cascade operation but were analyzed thoroughly in independent measurements.

2.3. Electrochemical Measurements. The first-stage electrolyzer was a custom-designed two-compartment polycarbonate cell with a large Ag-NC working electrode geometric surface area (~11 cm^2), a Pt mesh counter electrode, and a Ag/AgCl (3 M KCl) reference electrode. An anion exchange membrane (Selemion AMV) separated the Ag-NC cathode and reference from the Pt anode with 0.1 M $KHCO_3$ (pH 6.8) electrolyte in both chambers. The second-stage electrolysis cell was a similar two-compartment polycarbonate cell designed to maximize catalyst area relative to the electrolyte volume, enabling higher sensitivity for liquid product detection [32, 47]. An OD-Cu foil working electrode of ~5 cm^2 geometric surface area was used along with a Ag/AgCl (3 M KCl) reference electrode in the cathode compartment and a Pt mesh counter electrode in the anode compartment. The same Selemion anion exchange material was used as a membrane but with 0.1 M KOH electrolyte, in accord with the reported optimum electrolyte for CO reduction [46]. Electrochemical measurements were performed with either one (for an individual electrolyzer) or two (for the two-step cascade) Biologic SP-200 potentiostats. Potentiostatic electrochemical impedance spectroscopy measurements were performed before every experiment to determine the uncompensated cell resistance, R_u, and the potentiostat subsequently compensated for 85% of R_u in each cell during electrolysis. Potentials were converted to the reversible hydrogen electrode (RHE) utilizing the Nernst equation according to $V_{RHE} = V_{Ag/AgCl} + 0.210 + 0.059*pH_{soln}$ [48].

2.4. Product Quantification. Gaseous products were measured by gas chromatography (GC, SRI 8610) and liquid products were measured with nuclear magnetic resonance (NMR, Bruker 400

MHz) spectroscopy. Both the liquid and gas phase product concentrations were determined using calibrations from known standards. The gas phase products were injected into the GC via automatic valve injection (1 mL sample) with a thermal conductivity detector (TCD) and a flame ionization detector (FID). Nitrogen (99.99% Specialty Gases) was utilized as a carrier gas to permit accurate hydrogen quantification. For potentiostatic measurements, an injection to the GC was made after 5 min and then after each subsequent 30 min. Liquid samples for ^{1}H NMR spectroscopy were taken periodically throughout the experiment and at the end of each experiment. Samples were prepared by mixing D_2O and electrolyte aliquots in a 1:1 volume ratio. Dimethyl sulfoxide (DMSO) was added at a known low concentration for internal calibration.

Faradaic efficiency was calculated for the potentiostatic measurements by determining the charge required to produce the measured product concentration and dividing by the total charge passed during the time the sample underwent electrolysis. For the two-stage cascade experiments, the faradaic efficiency of ethanol was defined from CO_2 to C_2H_5OH across the entire system, as the charge required to produce the measured C_2H_5OH from CO_2 (12 mol e^- required per mol C_2H_5OH) divided by the sum of the charge passed in both electrolysis cells.

3. Results and Discussion

3.1. Individual Electrolyzer Performance. The two electrolysis reactors were first characterized independently to establish their expected performance characteristics and to identify the optimal operating conditions for their combination in a cascade system. Figure 2 shows the surface of each electrocatalyst, which displayed the expected morphology of the nanoporous coral-like structure for the Ag-NC catalyst [45] and the rough nanoparticulate surface of the OD-Cu [46].

Corresponding X-ray diffraction (XRD) data for each catalyst compared to an unaltered polycrystalline metal foil is shown in Figure S1. Double-layer capacitance measurements (Fig. S2) were used to estimate a roughness factor of 47 for Ag-NC and 196 for OD-Cu, based on electrochemically active surface area (Table S1). Figure 3 shows the faradaic efficiency of the reaction products for each electrolyzer as a function of applied potential, as well as the product distribution vs. time for the applied bias which resulted in the maximum faradaic efficiency for the desired product (i.e., CO for the first electrolyzer, C_2H_5OH for the second electrolyzer). Using the upstream CO_2 absorption column (see Experimental) to feed CO_2-saturated 0.1 M $KHCO_3$ to the Ag-NC electrocatalyst, a peak faradaic efficiency of 80% was achieved for CO at -0.6 V vs. RHE (Fig. 3a) at ~2.5 mA cm^{-2}. In the absence of CO_2, hydrogen was the only product detected (Fig. S3). The CO production performance at this potential was quite steady for CO_2 electroreduction, dropping only ~2% over > 1 h (Fig. 3c). The observed peak CO faradaic efficiency was lower than the 95% reported previously, which was attributed to supplying the CO_2 feedstock exclusively as a dissolved gas without active bubbling in the catholyte in contrast to previous work [45]. In the absence of active reactant gas bubbling across the electrocatalyst surface, CO_2 mass transport limitations arise which inhibit CO formation and permit greater hydrogen evolution instead. Despite the slight reduction in CO faradaic efficiency, the CO_2 absorption column was employed to minimize the concentration of CO_2 entering the outlet gas stream from the Ag-NC cathode chamber. The cathode outlet gas flow rate was measured to be 1.2 sccm, which was due to production of CO/H_2 gas. No CO_2 was detected in this outlet flow by GC. To independently test the second electrolyzer, pure CO (> 99.9%) was bubbled at 20 sccm below the OD-Cu electrocatalyst in the 0.1 M KOH catholyte. A peak faradaic efficiency for ethanol of 40% occurred at -0.3 V vs. RHE at ~1.8 mA cm^{-2}, with 12% for acetic acid and ~1%

ethylene (Fig. 3b). Monitoring performance at this operating potential vs. time, marginally higher CO reduction values and lower hydrogen was observed (some trace ethane was measured over time as well, Fig. 3d).

3.2. Cascade Electrolysis System Performance. After establishing the first- and second-stage electrolyzer operating potentials for optimal faradaic efficiency, the full cascade system was assembled and measured following the layout in Fig. 1. CO_2-saturated electrolyte was circulated through the cathode of the first electrolyzer, and the product CO/H_2 gases were bubbled into the second electrolyzer under the pressure created by their evolution during the electrochemical reaction. Separate potentiostats held the independent operating potentials for each electrolyzer and monitored the current density throughout the reaction. Figure 4 shows the current density vs. potential behavior of the first-stage (Ag-NC, 0.1 M $KHCO_3$) and second-stage (OD-Cu, 0.1 M KOH) electrolyzers as well as the current density vs. time for the experiment. Without active bubbling of CO_2 in the first cell, which was necessary to exclude CO_2 from the second stage, the circulation of electrolyte was important to improve the hydrodynamics of the cell through convection. At the first-stage operating potential of -0.6 V vs. RHE, an initial partial current density for CO formation of ~ 2 mA cm^{-2} was attained. Because of the low solubility of CO_2 and corresponding diffusion limitations, the increasing current density at more cathodic potentials can be largely attributed to an increasing partial current density for H_2 formation. After an initial drop in current density, the two electrolyzers at these operating potentials reached steady state current densities of comparable magnitude (~ 1 – 2 mA cm^{-2}, Fig. 4b). The higher initial current density from the OD-Cu may be attributable to the reduction of a surface oxide which remained despite the catalyst pretreatment.

Table 1 shows the system parameters and product faradaic efficiency measured for the

two-step cascade electrolysis. The output of the first cell was difficult to sample without interrupting the behavior of the cascade, so the CO faradaic efficiency in the output was assumed equal to that measured in the independently operated Ag-NC electrolyzer, which was observed to have quite steady performance over the time period of the cascade measurement (Fig. 3). A liquid aliquot of the second electrolyzer catholyte was collected after 40 min of operation and analyzed by NMR to determine the ethanol concentration. Based on the charge passed in the second cell only, the average C_2H_5OH faradaic efficiency was 28.4%. This result is less than the 42% measured for the individual OD-Cu electrolyzer with pure CO feedstock (Fig. 3), which was attributed to the ~20% H_2 content in the gas stream to the second cell of the cascade, as examined further below. The average total faradaic efficiency for C_2H_5OH was 11.0% based on the total charge passed between both electrolyzers in the cascade.

The cascade electrolysis faradaic efficiency for CO2RR to ethanol of 11.0% is not as high as has been reported for some other systems at high applied potential (Table 2), but it compares favorably to state-of-the-art catalysts at modest cathodic potential (~ -0.5 V vs. RHE) [33-38]. Comparison of the overpotential for ethanol formation between a single electrolysis step and the cascade system is complicated by having two different operating potentials in the two-step electrolysis. Although the two electrolyzers are connected in series for the chemical flow, they are independent electrical loads. Rather than additive voltages as would occur in electrical series, the overall cascade system effective applied potential for CO_2 conversion to C_2H_5OH is a charge-weighted average of the two electrolyzer applied potentials. The electrolyzer efficiency depends on the energy stored in the ethanol relative to the total electrical energy required to produce it, and the total cascade power consumption is the sum of the two electrolysis cell powers at their respective operating currents and applied voltages. Thus, a single effective applied potential for

the cascade can be determined for comparison purposes by averaging the individual cell applied potentials weighted by the charge passed in each. Ideally in the absence of side reactions, the net potential in the cascade system for the 12 electrons needed to convert 2 CO_2 molecules to C_2H_5OH (Eqn. 1) is the weighted average of the applied potential in the first stage for the 4 electrons needed to make 2 CO molecules (Eqn. 2) and the applied potential in the second stage for the 8 electrons needed to convert the 2 CO molecules to C_2H_5OH (Eqn. 3). For the reported cascade system operating potentials herein, this net potential would be -0.4 V vs. RHE, corresponding to a cathodic overpotential of ~490 mV for ethanol production (Eqn. 1). Practically, for a system with byproducts and less than perfect conversion of the intermediate product (i.e., CO), the average system applied potential should be weighted by the total charge passed in each electrolysis step. For the reported two-step cascade, this average system operating potential is -0.52 V vs. RHE, corresponding to a cathodic overpotential of ~610 mV for ethanol production.

One of the significant limitations of this cascade system in its current design was poor conversion of the CO intermediate to C_2H_5OH. Comparing the measured ethanol product to the projected CO formation rate from the individual first-stage electrolyzer measurements, this conversion rate was estimated to be only 6.4% (Table 1). The extra charge wasted to generate unconverted CO lowered the overall cascade C_2H_5OH faradaic efficiency and increased the average cascade overpotential as well. The low solubility of CO in water is assumed to be a major contributor to this poor CO conversion rate [46]. CO gas bubbles introduced to the second electrolyzer were observed to pass through the catholyte without full dissolution. Significant improvements to the CO conversion and the resulting cascade C_2H_5OH faradaic efficiency are thus expected for a future reactor design spreading the intermediate CO gas flow to the second

electrolyzer in smaller bubbles across a larger area OD-Cu cathode in a greater electrolyte volume. Alternatively, a separator to remove CO from H_2 in the second electrolyzer gas output and recycle it back to the OD-Cu cathode gas input stream is expected to strongly increase the CO conversion and subsequent cascade performance. On an industrial scale, pressure swing adsorption is a viable cost-effective technology for achieving this separation, which has been shown to be an insignificant expense in the technoeconomic analysis for electrochemical CO_2 reduction [49]. If a recycle stream or modified reactor design allowed complete conversion of the CO intermediate while maintaining the other system performance characteristics (Table 1, 80% faradaic efficiency for CO at -0.6 V vs. RHE in electrolyzer 1, 28.4% faradaic efficiency for C_2H_5OH at -0.3 V vs. RHE in electrolyzer 2 with 7.4% faradaic efficiency for acetate, with the balance towards H_2), an overall cascade faradaic efficiency for C_2H_5OH of 33.4% would be predicted at an average applied potential of -0.36 V vs. RHE (see SI). Furthermore, if state-of-the-art CO_2-to-CO (98% faradaic efficiency with Ag in ionic liquid at ~ -0.25 V vs. RHE [50]) and CO-to-C_2H_5OH (42% faradaic efficiency for ethanol with 11% faradaic efficiency for acetate, with the balance towards H_2 with OD-Cu in 0.1 M KOH at -0.3 V vs. RHE [46]) electrochemical conversion performance characteristics were combined with 100% CO conversion in a perfect recycle stream, an overall cascade faradaic efficiency of 47.5% would be predicted with an average applied potential of -0.29 V vs. RHE (~380 mV overpotential)(see SI). Additionally, the highest reported single electrocatalyst conversions of CO_2 to C_2H_5OH to date have relied on highly nanostructured architectures of Cu [36, 39]. Because the C-C bond formation step is predicted to occur from hydrogenated adsorbed *CO species rather than CO_2 [51], it could be expected that increased CO faradaic efficiency to C_2H_5OH could similarly result with these nanostructured catalysts. And because Cu is not the ideal binding energy surface for

the conversion of CO_2 to CO, a cascade approach with an optimized first stage to produce CO should thus outperform the single catalyst system with lower overall overpotential. Thus, reactor design improvements to the cascade system have the capability of leading to a significant improvement in CO_2-to-C_2H_5OH electrochemical conversion.

While a high selectivity to C_2H_5OH in the second-stage electrolyzer with OD-Cu was confirmed with a pure CO feed (Fig. 3b), the presence of CO_2 and/or H_2 was expected to introduce competing reactions which could reduce the faradaic efficiency for ethanol formation. The CO_2 absorption column was thus incorporated into the cascade system upstream of the first-stage electrolyzer to prevent excess non-dissolved CO_2 from carrying over to the second reactor. The effect of CO_2/H_2 in the feed to the second cell was simulated using a controlled gas mixture in an individual measurement on the OD-Cu system (Fig. 5a). Using a 4:1 CO:H_2 (no CO_2) gas flow in accordance with the expected product from the first stage, the OD-Cu cathode displayed 28% faradaic efficiency for C_2H_5OH after 40 min, with significantly reduced acetate production compared to a pure CO feed. Furthermore, dilution of this mixed flow with 5% CO_2 by volume decreased the ethanol faradaic efficiency to 5%, which dropped to < 3% at 10% CO_2, and acetate was no longer detected as a side product. Thus, exclusion of CO_2 from the second cell catholyte was deemed critical to performance. Furthermore, with the 4:1 CO:H_2 (no CO_2) gas flow composition, the faradaic efficiency for ethanol was observed to be time-dependent. As shown in Figure 5b, the cumulative C_2H_5OH faradaic efficiency decreased with time beyond 30 min.

As seen in Figure 6, analysis of the catholyte from the second electrolyzer with NMR showed that the initially strong peaks for ethanol were greatly reduced after > 1 h. The loss of the ethanol peaks coincided with the appearance of new NMR peaks. Taken after 30 min of cascade system operation, peaks for ethanol were clearly evident at a chemical shift of 1.0 and 3.5 ppm.

After 1 h, the ethanol signal was largely replaced with new peaks at 1.4, 2.2, 7.0 and 7.8 ppm. Definitive assignment of these peaks was elusive and remains a subject of future efforts, but the lower two peaks are possibly consistent with the presence of propionaldehyde, a three-carbon (C_3) species that has previously been observed in small amounts as a product of CO_2 reduction on copper cathodes [18]. Ethyl acetate, a four-carbon species, is also a possibility. The origin of the other two peaks at 7 – 8 ppm is presently unclear, although in the absence of nitrogen bonding, peaks in this range for ^{1}H NMR are generally attributed to aromatic compounds [52]. It can thus be inferred that in the presence of CO/H_2 at reductive potentials in the second electrolyzer, the C_2H_5OH was further reduced to C_{3+} species, resulting in the shift in the NMR signal. For a sustainable cascade system optimized for ethanol production, the liquid catholyte of the second-stage electrolyzer should therefore be continually cycled through a separator to isolate the C_2H_5OH product before further reaction.

4. Conclusion

A two-stage, heterogeneously catalyzed electrochemical cascade reactor was constructed and tested to convert CO_2 to CO to C_2H_5OH. Despite the present cascade design's low conversion of CO between electrolyzer 1 and 2, a competitive overall cascade faradaic efficiency for ethanol of 11.0% was achieved at an average applied potential of -0.52 V vs. RHE. Gaseous CO_2 was excluded from the electrolyzers using an upstream absorption column because the presence of small quantities of CO_2 in the second electrolyzer was measured to strongly impede the production of ethanol. The primary advantage of this multistage cascade electrolysis approach is its versatility and modularity. With a stable intermediate species between reactors (e.g., CO in this work), each electrochemical conversion step can be optimized for maximum

faradaic efficiency and minimum overpotential by independently controlling the operating parameters. The two electrolyzers employed in the cascade system of this work operated simultaneously with different applied biases, electrolytes, and electrocatalysts. The cascade approach thus holds promise as a generic strategy to achieve higher selectivity for the electrochemical synthesis of more complex products. For the present CO_2 to CO to C_2H_5OH approach, a better reactor design with separation and recycle streams to maximize the CO conversion and prevent further C_2H_5OH reduction was predicted to enable a faradaic efficiency for ethanol from carbon dioxide up to 47.5% at an average cathodic overpotential < 400 mV. The cascade route demonstrated herein could thus help advance the practicality of converting waste CO_2 into a useful liquid fuel such as ethanol.

Acknowledgements

The authors acknowledge financial support from the Kentucky Department for Energy Development and Independence grant #PON2 127 1500002410. The authors also acknowledge support from the Conn Center for Renewable Energy Research at the University of Louisville.

Supporting Information

Projected cascade system performance calculations. This material is available free of charge via the Internet at http://pubs.acs.org.

References

[1] N.S. Lewis, D.G. Nocera, Powering the planet: Chemical challenges in solar energy utilization, Proc. Natl. Acad. Sci. U. S. A., 103 (2006) 15729-15735.

[2] M. Gratzel, Artificial Photosynthesis - Water Cleavage into Hydrogen and Oxygen by Visible-Light, Acc. Chem. Res., 14 (1981) 376-384.

[3] A.J. Bard, M.A. Fox, Artificial Photosynthesis - Solar Splitting of Water to Hydrogen and Oxygen, Acc. Chem. Res., 28 (1995) 141-145.

[4] J.J. Eberhart, Fuels of the Future for Cars and Trucks, Energy Efficiency and Renewable Energy, U.S. Department of Energy - 2002 Diesel Engine Emissions Reduction (DEER) Workshop, San Diego, CA, 2002.

[5] Gurudayal, J. Bullock, D.F. Sranko, C.M. Towle, Y.W. Lum, M. Hettick, M.C. Scott, A. Javey, J. Ager, Efficient solar-driven electrochemical CO2 reduction to hydrocarbons and oxygenates, Energy Environ. Sci., 10 (2017) 2222-2230.

[6] K.R. Rao, S. Pishgar, J. Strain, B. Kumar, V. Atla, S. Kumari, J.M. Spurgeon, Photoelectrochemical reduction of CO2 to HCOOH on silicon photocathodes with reduced SnO2 porous nanowire catalysts, Journal of Materials Chemistry A, 6 (2018) 1736-1742.

[7] R. Kuriki, H. Matsunaga, T. Nakashima, K. Wada, A. Yamakata, O. Ishitani, K. Maeda, Nature-Inspired, Highly Durable CO2 Reduction System Consisting of a Binuclear Ruthenium(II) Complex and an Organic Semiconductor Using Visible Light, J. Am. Chem. Soc., 138 (2016) 5159-5170.

[8] S.B. Wang, X.C. Wang, Imidazolium Ionic Liquids, Imidazolylidene Heterocyclic Carbenes, and Zeolitic Imidazolate Frameworks for CO2 Capture and Photochemical Reduction, Angew. Chem.-Int. Edit., 55 (2016) 2308-2320.

[9] R. Kuriki, M. Yamamoto, K. Higuchi, Y. Yamamoto, M. Akatsuka, D. Lu, S. Yagi, T. Yoshida, O. Ishitani, K. Maeda, Robust Binding between Carbon Nitride Nanosheets and a Binuclear Ruthenium(II) Complex Enabling Durable, Selective CO2 Reduction under Visible Light in Aqueous Solution, Angew. Chem.-Int. Edit., 56 (2017) 4867-4871.

[10] S.B. Wang, W.S. Yao, J.L. Lin, Z.X. Ding, X.C. Wang, Cobalt Imidazolate Metal-Organic Frameworks Photosplit CO2 under Mild Reaction Conditions, Angew. Chem.-Int. Edit., 53 (2014) 1034-1038.

[11] S.B. Wang, B.Y. Guan, Y. Lu, X.W. Lou, Formation of Hierarchical In2S3-CdIn2S4 Heterostructured Nanotubes for Efficient and Stable Visible Light CO2 Reduction, J. Am. Chem. Soc., 139 (2017) 17305-17308.

[12] B. Kumar, M. Llorente, J. Froehlich, T. Dang, A. Sathrum, C.P. Kubiak, Photochemical and Photoelectrochemical Reduction of CO2, Annual Review of Physical Chemistry, Vol 63, 63 (2012) 541-569.

[13] S.C. Roy, O.K. Varghese, M. Paulose, C.A. Grimes, Toward Solar Fuels: Photocatalytic Conversion of Carbon Dioxide to Hydrocarbons, ACS Nano, 4 (2010) 1259-1278.

[14] J. Qiao, Y. Liu, F. Hong, J. Zhang, A review of catalysts for the electroreduction of carbon dioxide to produce low-carbon fuels, Chem. Soc. Rev., 43 (2014) 631-675.

[15] H. Noda, S. Ikeda, Y. Oda, K. Imai, M. Maeda, K. Ito, Electrochemical Reduction of Carbon Dioxide at Various Metal Electrodes in Aqueous Potassium Hydrogen Carbonate Solution, Bull. Chem. Soc. Jpn., 63 (1990) 2459-2462.

[16] Y. Hori, K. Kikuchi, S. Suzuki, Production of CO and CH_4 in Electrochemical Reduction of CO_2 at Metal Electrodes in Aqueous Hydrogencarbonate Solution, Chem. Lett., (1985) 1695-1698.

[17] Y. Hori, K. Kikuchi, A. Murata, S. Suzuki, Production of Methane and Ethylene in Electrochemical Reduction of Carbon Dioxide at Copper Electrodes in Aqueous Hydrogencarbonate Solution, Chem. Lett., (1986) 897-898.

[18] K.P. Kuhl, E.R. Cave, D.N. Abram, T.F. Jaramillo, New insights into the electrochemical reduction of carbon dioxide on metallic copper surfaces, Energy Environ. Sci., 5 (2012) 7050-7059.

[19] M. Gattrell, N. Gupta, A. Co, A review of the aqueous electrochemical reduction of CO2 to hydrocarbons at copper, J. Electroanal. Chem., 594 (2006) 1-19.

[20] Y. Hori, A. Murata, R. Takahashi, Formation of Hydrocarbons in the Electrochemical Reduction of Carbon-Dioxide at a Copper Electrode in Aqueous Solution, Journal of the Chemical Society-Faraday Transactions I, 85 (1989) 2309-2326.

[21] A.A. Peterson, F. Abild-Pedersen, F. Studt, J. Rossmeisl, J.K. Norskov, How copper catalyzes the electroreduction of carbon dioxide into hydrocarbon fuels, Energy Environ. Sci., 3 (2010) 1311-1315.

[22] T. Hatsukade, K.P. Kuhl, E.R. Cave, D.N. Abram, T.F. Jaramillo, Insights into the electrocatalytic reduction of CO2 on metallic silver surfaces, PCCP, 16 (2014) 13814-13819.

[23] Y. Chen, C.W. Li, M.W. Kanan, Aqueous CO2 Reduction at Very Low Overpotential on Oxide-Derived Au Nanoparticles, J. Am. Chem. Soc., 134 (2012) 19969-19972.

[24] M. Asadi, B. Kumar, A. Behranginia, B.A. Rosen, A. Baskin, N. Repnin, D. Pisasale, P. Phillips, W. Zhu, R. Haasch, R.F. Klie, P. Kral, J. Abiade, A. Salehi-Khojin, Robust carbon dioxide reduction on molybdenum disulphide edges, Nat. Commun., 5 (2014) 4470-4470.

[25] C. Delacourt, P.L. Ridgway, J.B. Kerr, J. Newman, Design of an electrochemical cell making syngas (CO+H-2) from CO2 and H2O reduction at room temperature, J. Electrochem. Soc., 155 (2008) B42-B49.

[26] A.S. Agarwal, Y. Zhai, D. Hill, N. Sridhar, The Electrochemical Reduction of Carbon Dioxide to Formate/Formic Acid: Engineering and Economic Feasibility, Chemsuschem, 4 (2011) 1301-1310.

[27] C.W. Li, M.W. Kanan, CO2 Reduction at Low Overpotential on Cu Electrodes Resulting from the Reduction of Thick Cu2O Films, J. Am. Chem. Soc., 134 (2012) 7231-7234.

[28] J. Qiao, P. Jiang, J. Liu, J. Zhang, Formation of Cu nanostructured electrode surfaces by an annealing-electroreduction procedure to achieve high-efficiency CO2 electroreduction, Electrochem. Commun., 38 (2014) 8-11.

[29] T. Sekimoto, M. Deguchi, S. Yotsuhashi, Y. Yamada, T. Masui, A. Kuramata, S. Yamakoshi, Highly selective electrochemical reduction of CO2 to HCOOH on a gallium oxide cathode, Electrochem. Commun., 43 (2014) 95-97.

[30] J. Wu, F.G. Risalvato, F.-S. Ke, P.J. Pellechia, X.-D. Zhou, Electrochemical Reduction of Carbon Dioxide I. Effects of the Electrolyte on the Selectivity and Activity with Sn Electrode, J. Electrochem. Soc., 159 (2012) F353-F359.

[31] F. Koleli, D. Balun, Reduction of CO2 under high pressure and high temperature on Pb-granule electrodes in a fixed-bed reactor in aqueous medium, Applied Catalysis a-General, 274 (2004) 237-242.

[32] B. Kumar, V. Atla, J.P. Brian, S. Kumari, T.Q. Nguyen, M. Sunkara, J.M. Spurgeon, Reduced SnO2 Porous Nanowires with a High Density of Grain Boundaries as Catalysts for Efficient Electrochemical CO2-into-HCOOH Conversion, Angew. Chem.-Int. Edit., 56 (2017) 3645-3649.

[33] D. Ren, B.S.H. Ang, B.S. Yeo, Tuning the Selectivity of Carbon Dioxide Electroreduction toward Ethanol on Oxide-Derived CuxZn Catalysts, ACS Catal., 6 (2016) 8239-8247.

[34] Y. Hori, I. Takahashi, O. Koga, N. Hoshi, Electrochemical reduction of carbon dioxide at various series of copper single crystal electrodes, Journal of Molecular Catalysis a-Chemical, 199 (2003) 39-47.

[35] D. Ren, Y.L. Deng, A.D. Handoko, C.S. Chen, S. Malkhandi, B.S. Yeo, Selective Electrochemical Reduction of Carbon Dioxide to Ethylene and Ethanol on Copper(I) Oxide Catalysts, ACS Catal., 5 (2015) 2814-2821.

[36] T.T.H. Hoang, S.C. Ma, J.I. Gold, P.J.A. Kenis, A.A. Gewirth, Nanoporous Copper Films by Additive-Controlled Electrodeposition: CO2 Reduction Catalysis, ACS Catal., 7 (2017) 3313-3321.

[37] S.C. Ma, M. Sadakiyo, R. Luo, M. Heima, M. Yamauchi, P.J.A. Kenis, One-step electrosynthesis of ethylene and ethanol from CO2 in an alkaline electrolyzer, J. Power Sources, 301 (2016) 219-228.

[38] A.D. Handoko, C.W. Ong, Y. Huang, Z.G. Lee, L.Y. Lin, G.B. Panetti, B.S. Yeo, Mechanistic Insights into the Selective Electroreduction of Carbon Dioxide to Ethylene on Cu2O-Derived Copper Catalysts, J. Phys. Chem. C, 120 (2016) 20058-20067.

[39] Y. Song, R. Peng, D.K. Hensley, P.V. Bonnesen, L.B. Liang, Z.L. Wu, H.M. Meyer, M.F. Chi, C. Ma, B.G. Sumpter, A.J. Rondinone, High-Selectivity Electrochemical Conversion of CO2 to Ethanol using a Copper Nanoparticle/N-Doped Graphene Electrode, Chemistryselect, 1 (2016) 6055-6061.

[40] Y.G. Kim, A. Javier, J.H. Baricuatro, D. Torelli, K.D. Cummins, C.F. Tsang, J.C. Hemminger, M.P. Soriaga, Surface reconstruction of pure-Cu single-crystal electrodes under CO-reduction potentials in alkaline solutions: A study by seriatim ECSTM-DEMS, J. Electroanal. Chem., 780 (2016) 290-295.

[41] Z.W. Seh, J. Kibsgaard, C.F. Dickens, I.B. Chorkendorff, J.K. Norskov, T.F. Jaramillo, Combining theory and experiment in electrocatalysis: Insights into materials design, Science, 355 (2017) 146.

[42] C.A. Huff, M.S. Sanford, Cascade Catalysis for the Homogeneous Hydrogenation of CO2 to Methanol, J. Am. Chem. Soc., 133 (2011) 18122-18125.

[43] Y. Chen, S. Choi, L.T. Thompson, Low-Temperature CO2 Hydrogenation to Liquid Products via a Heterogeneous Cascade Catalytic System, ACS Catal., 5 (2015) 1717-1725.

[44] B. Kumar, J.P. Brian, V. Atla, S. Kumari, K.A. Bertram, R.T. White, J. Spurgeon, New trends in the development of heterogeneous catalysts for electrochemical CO2 reduction, Catal. Today, 270 (2016) 19-30.

[45] Y.C. Hsieh, S.D. Senanayake, Y. Zhang, W.Q. Xu, D.E. Polyansky, Effect of Chloride Anions on the Synthesis and Enhanced Catalytic Activity of Silver Nanocoral Electrodes for CO2 Electroreduction, ACS Catal., 5 (2015) 5349-5356.

[46] C.W. Li, J. Ciston, M.W. Kanan, Electroreduction of carbon monoxide to liquid fuel on oxide-derived nanocrystalline copper, Nature, 508 (2014) 504-507.

[47] B. Kumar, J.P. Brian, V. Atla, S. Kumari, K.A. Bertram, R.T. White, J.M. Spurgeon, Controlling the Product Syngas H-2:CO Ratio through Pulsed-Bias Electrochemical Reduction of CO2 on Copper, ACS Catal., 6 (2016) 4739-4745.

[48] A.J. Bard, L.R. Faulkner, Electrochemical Methods: Fundamentals and Applications, 2nd edition ed., John Wiley & Sons2001.

[49] X. Li, P. Anderson, H.-R.M. Jhong, M. Paster, J.F. Stubbins, P.J.A. Kenis, Greenhouse Gas Emissions, Energy Efficiency, and Cost of Synthetic Fuel Production Using Electrochemical CO_2 Conversion and the Fischer-Tropsch Process, Energy & Fuels, 30 (2016) 5980-5989.

[50] B.A. Rosen, A. Salehi-Khojin, M.R. Thorson, W. Zhu, D.T. Whipple, P.J.A. Kenis, R.I. Masel, Ionic Liquid-Mediated Selective Conversion of CO2 to CO at Low Overpotentials, Science, 334 (2011) 643-644.

[51] J.H. Montoya, A.A. Peterson, J.K. Norskov, Insights into CC Coupling in CO2 Electroreduction on Copper Electrodes, ChemCatChem, 5 (2013) 737-742.

[52] Handbook of Proton-NMR Spectra and Data, Academic Press, Inc., Orlando, FL, 1987.

Tables.

Table 1. Key parameters for the CO_2 to ethanol two-step cascade electrolysis.

First Electrolyzer			
Catalyst	**Electrolyte**	**Operating Potential**	**CO FE (%)[a]**
Ag-NC	0.1 M $KHCO_3$	-0.6 V vs. RHE	80
Second Electrolyzer			
Catalyst	**Electrolyte**	**Operating Potential**	**C_2H_5OH FE (%)[b]**
OD-Cu	0.1 M KOH	-0.3 V vs. RHE	28.4
Total Cascade Electrolyzer System			
CO to C_2H_5OH Conversion (%)		**Average Potential[c]**	**C_2H_5OH FE (%)[d]**
6.4		-0.52 V vs. RHE	11.0

[a] First-stage electrolyzer CO faradaic efficiency estimated from values determined at the same conditions for the independently measured Ag-NC system, with stability as seen in Figure 3c.

[b] Determined from ethanol content measured in the second electrolyzer after 40 min of cascade system operation, based on the charge passed at the OD-Cu only.

[c] Average applied potential across the two electrolyzers of the cascade, weighted by the charge passed in each electrolyzer.

[d] Determined from ethanol content measured in the second electrolyzer after 40 min of cascade system operation, based on the total charge passed between both electrolyzers.

Table 2. Literature reports of the performance of electroreduction of CO_2 to ethanol.

Catalyst	Electrolyte	Potential	C_2H_5OH FE (%)
polycrystalline Cu [18]	0.1 M $KHCO_3$	-1.05 V vs. RHE	9.8
Cu (100) [34]	0.1 M $KHCO_3$	-1.00 V vs. RHE	9.7
Cu (110) [34]	0.1 M $KHCO_3$	-1.18 V vs. RHE	10.5
Cu (111) [34]	0.1 M $KHCO_3$	-1.15 V vs. RHE	2.6
Cu (310) [34]	0.1 M $KHCO_3$	-1.02 V vs. RHE	29.9
Cu_2O microparticles on Cu [35]	0.1 M $KHCO_3$	-0.99 V vs. RHE	16.4
OD-Cu particles [38]	0.1 M $KHCO_3$	-0.98 V vs. RHE	11.8
Cu_4Zn film [33]	0.1 M $KHCO_3$	-1.05 V vs. RHE	29.1
Cu nanoparticles/N-doped graphene [39]	0.1 M $KHCO_3$	-1.20 V vs. RHE	63.0
Cu nanoparticles on GDE[a] [37]	1 M KOH	-0.80 V vs. RHE	17.0
CuDAT-wire[b] [36]	1 M KOH	-0.60 V vs. RHE	25.0
Ag-NC/OD-Cu Cascade[c]	0.1 M $KHCO_3$/0.1 M KOH[c]	-0.52 V vs. RHE[c]	11.0[c]

[a] Gas diffusion electrode (GDE)

[b] 3,5-diamino-1,2,4-triazole (DAT)

[c] The cascade system of this work, with Ag nanocoral (Ag-NC) in 0.1 M $KHCO_3$ in the first stage and oxide-derived Cu (OD-Cu) in 0.1 M KOH in the second stage. The average applied potential of the system as weighted by the charge passed in each stage, and the faradaic efficiency based on the charge passed in both stages.

Figure Captions

Figure 1. Schematic of the two-step CO_2-to-ethanol cascade electrolysis system.

Figure 2. SEM images with insets of (A) the Ag-NC catalyst of the first-stage electrolyzer and (B) OD-Cu of the second-stage electrolyzer.

Figure 3. Individual electrolyzer performance. Peak product faradaic efficiency for (A) the first electrolyzer with Ag-NC catalyst in 0.1 M $KHCO_3$ saturated with pure CO_2 and (B) the second electrolyzer with OD-Cu catalyst in 0.1 M KOH bubbled with pure CO. (C) Product faradaic efficiencies vs. time for the electrolyzer from (A) held at -0.6 V vs. RHE. (D) Product faradaic efficiencies vs. time for the electrolyzer from (B) held at -0.3 V vs. RHE.

Figure 4. Two-stage cascade performance. (A) Current density vs. potential for the first-stage (black curve) and second-stage (red curve) electrolyzers. (B) Current density vs. time for the cascade at potentiostatic operating conditions with the first cell at -0.6 V vs. RHE and the second cell at -0.3 V vs. RHE.

Figure 5. (A) Liquid product faradaic efficiencies for the second electrolyzer with varying flow composition. 5% and 10% CO_2 compositions had a balance of 4:1 $CO:H_2$. (B) Second electrolyzer ethanol faradaic efficiency vs. time with a 4:1 $CO:H_2$ feedstock.

Figure 6. NMR spectra for liquid products of the cascade electrolysis after operation for 30 min (green) and for 60 min (black). DMSO was used as an internal standard.

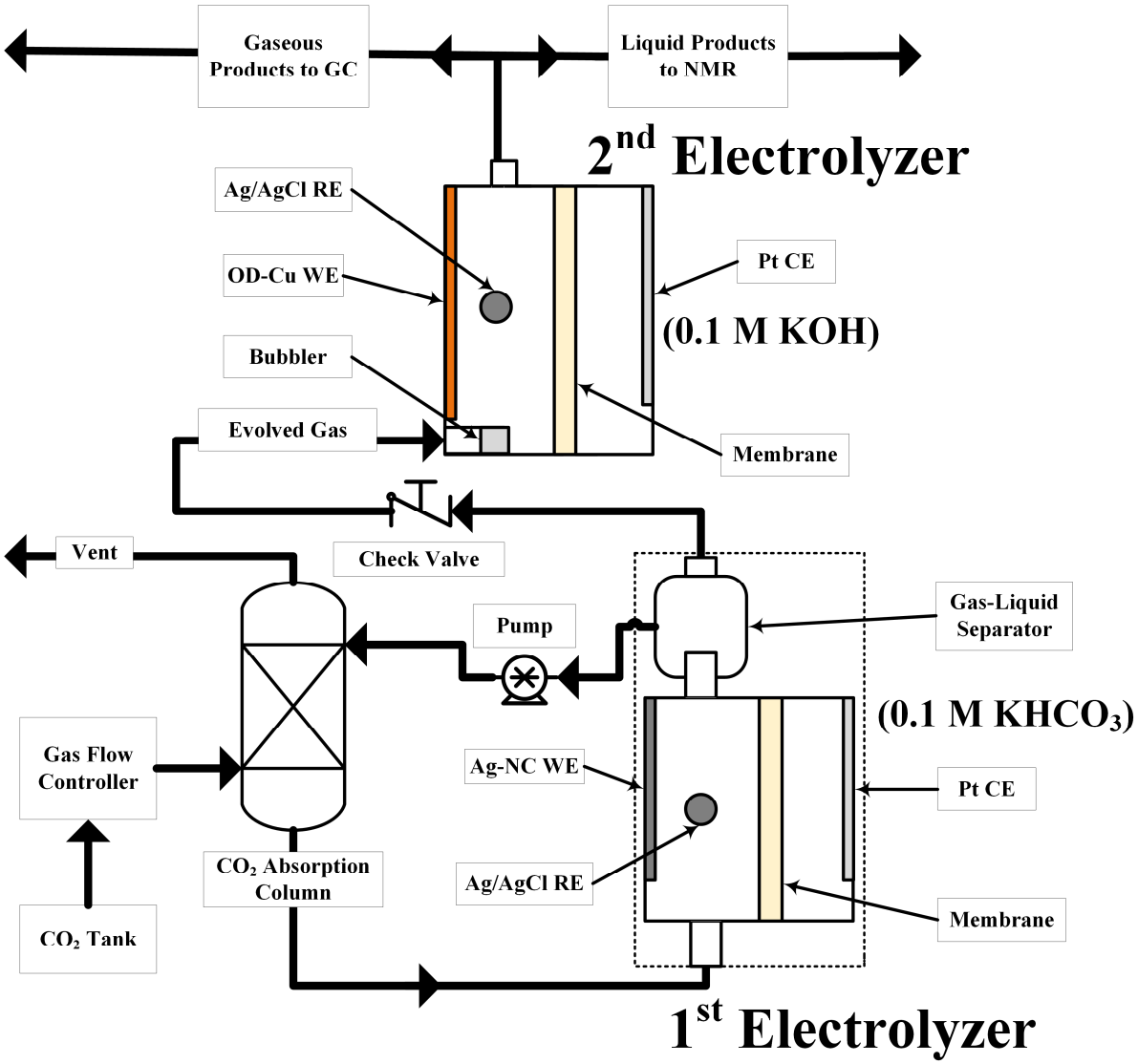
Gaseous Products to GC
Liquid Products to NMR
2nd Electrolyzer
Ag/AgCl RE
OD-Cu WE
Bubbler
Evolved Gas
Pt CE
(0.1 M KOH)
Membrane
Vent
Check Valve
Pump
Gas-Liquid Separator
(0.1 M KHCO3)
Gas Flow Controller
Ag-NC WE
Pt CE
CO2 Absorption Column
Ag/AgCl RE
Membrane
CO2 Tank
1st Electrolyzer

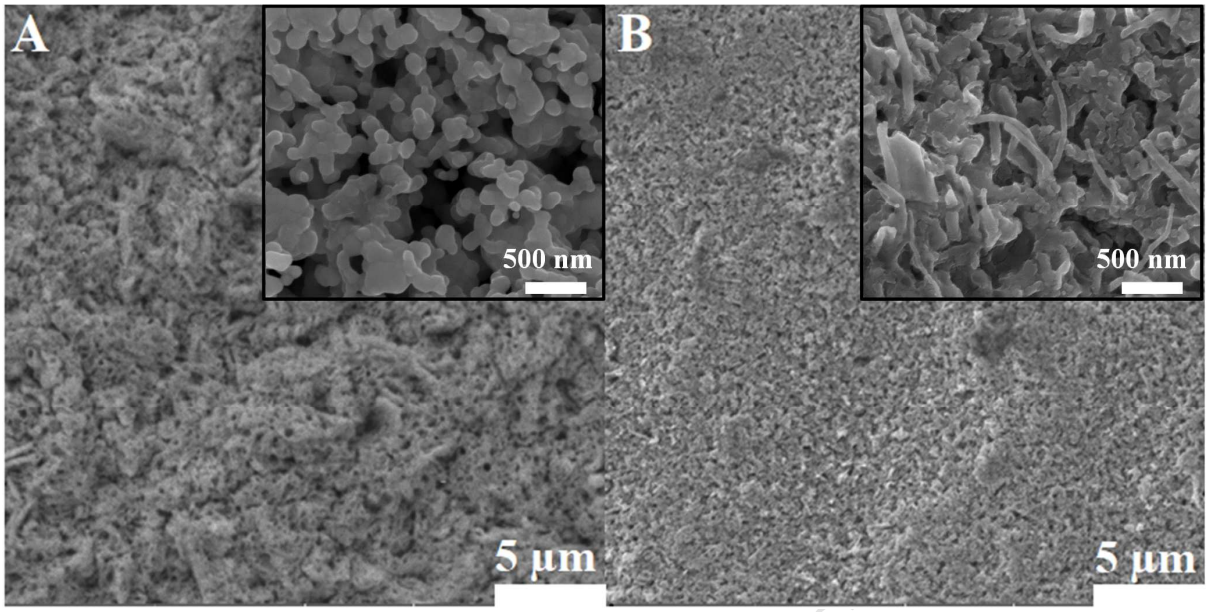

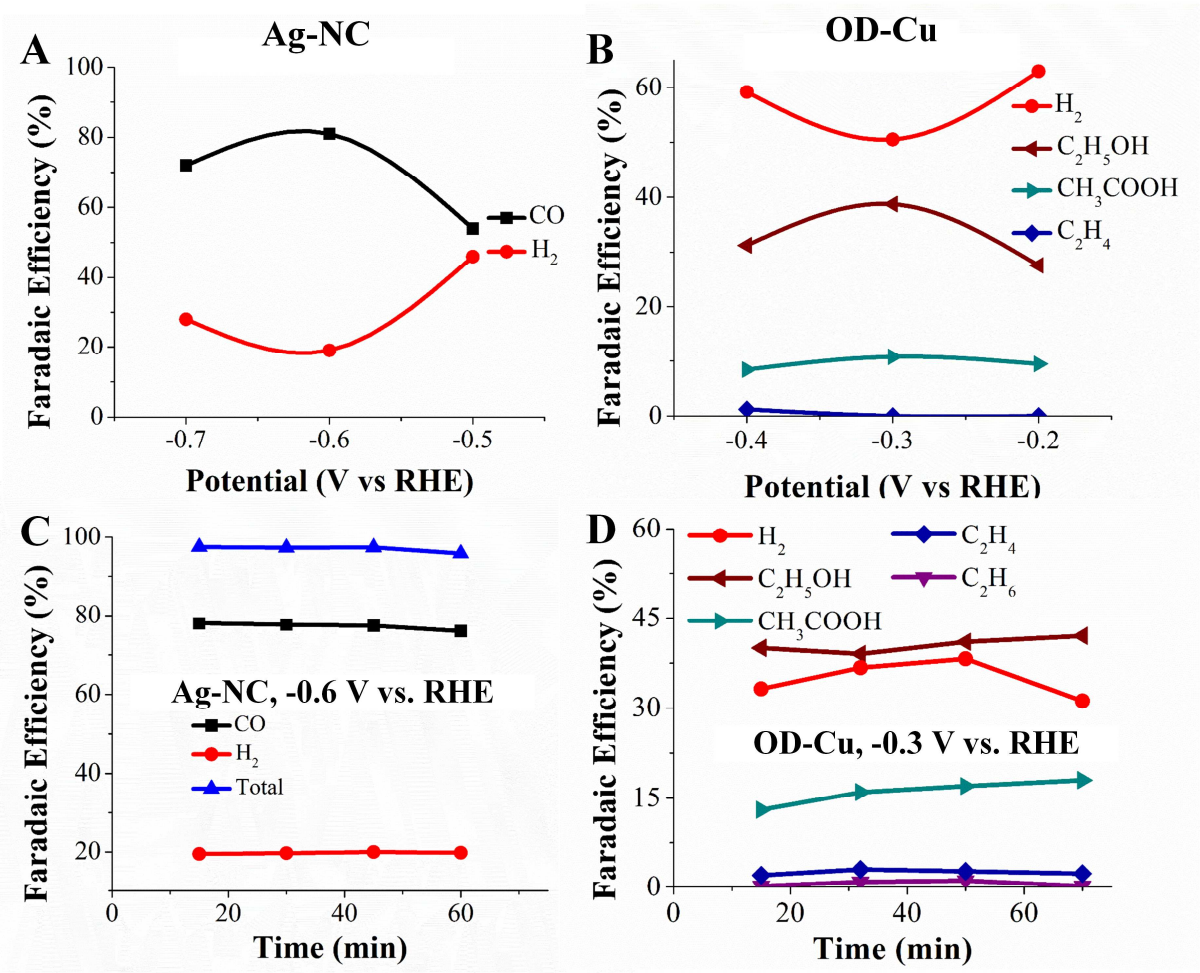
A
Ag-NC
Faradaic Efficiency (%)
Potential (V vs RHE)
CO
H2
B
OD-Cu
Faradaic Efficiency (%)
Potential (V vs RHE)
H2
C2H5OH
CH3COOH
C2H4
C
Ag-NC, -0.6 V vs. RHE
Faradaic Efficiency (%)
Time (min)
CO
H2
Total
D
OD-Cu, -0.3 V vs. RHE
Faradaic Efficiency (%)
Time (min)
H2
C2H4
C2H5OH
C2H6
CH3COOH

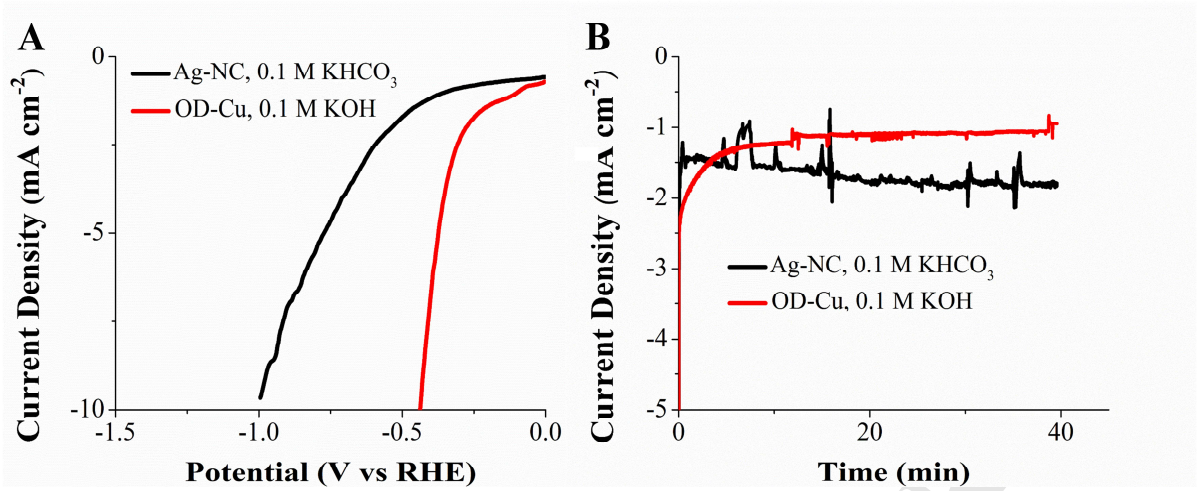

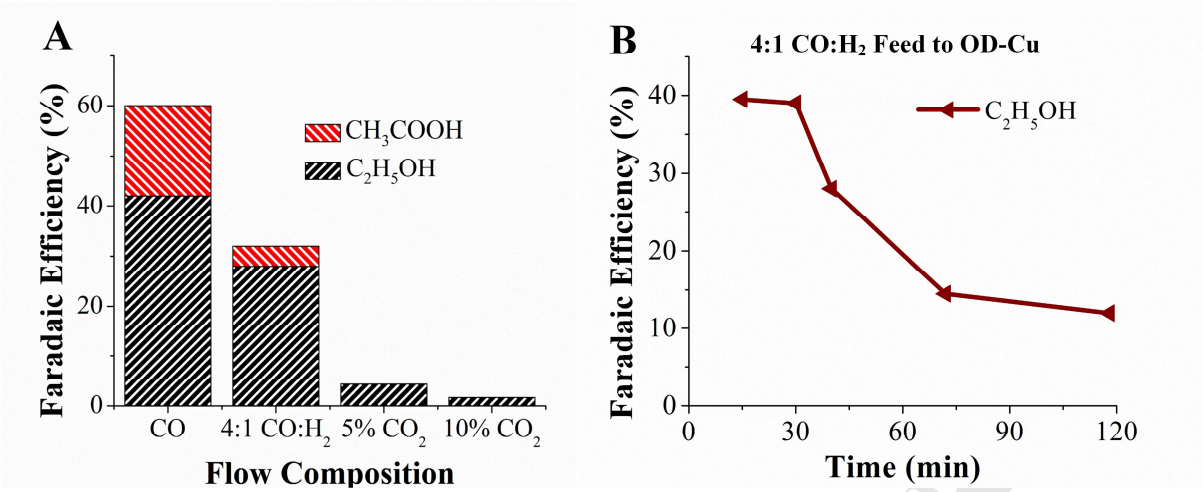

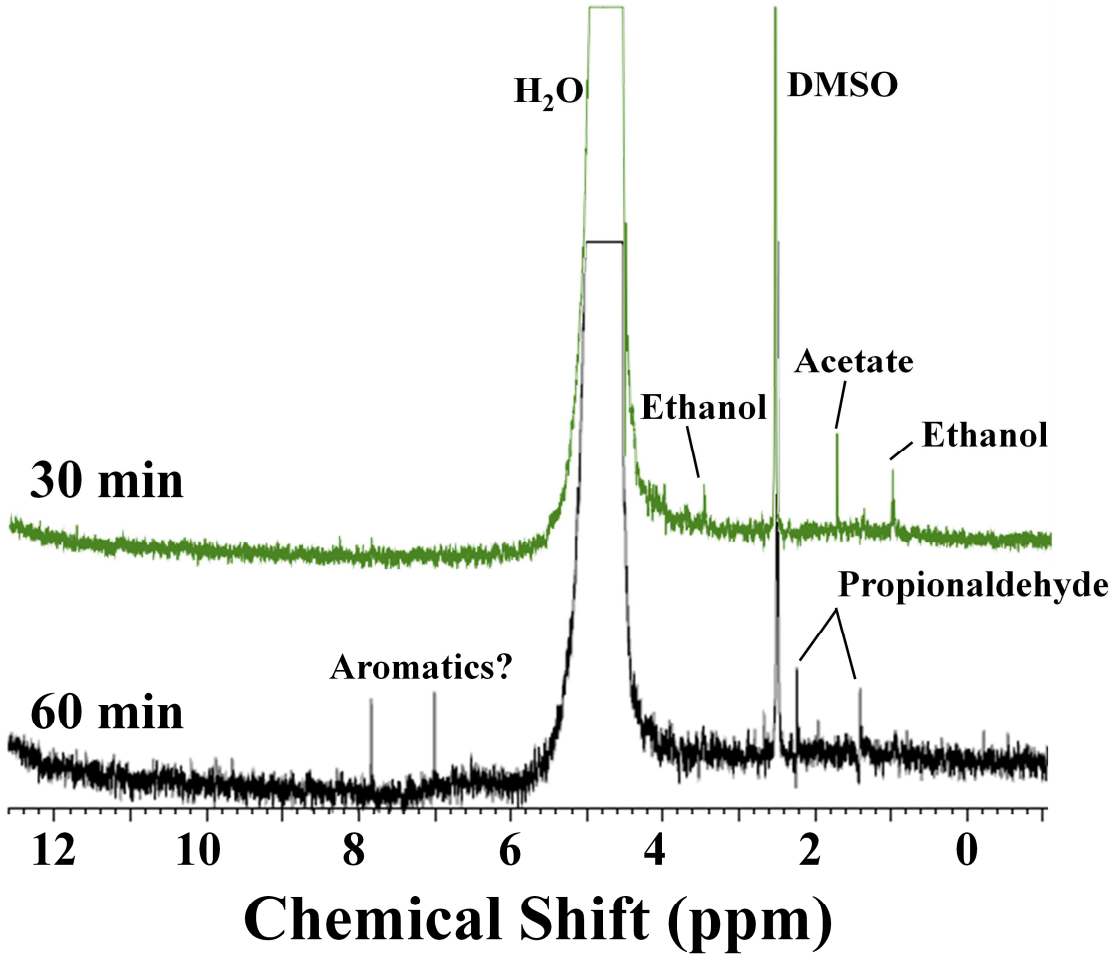
H2O
DMSO
Acetate
Ethanol
Ethanol
30 min
Propionaldehyde
Aromatics?
60 min
12
10
8
6
4
2
0
Chemical Shift (ppm)